On the effects of partial substitution of Co for Fe in FINEMET and Nb-containing HITPERM alloys

2003 J. Phys.: Condens. Matter 15 3957

(http://iopscience.iop.org/0953-8984/15/23/309)

INSTITUTE OF PHYSICS PUBLISHING JOURNAL OF PHYSICS: CONDENSED MATTER

J. Phys.: Condens. Matter **15** (2003) 3957–3968 PII: S0953-8984(03)59779-X

On the effects of partial substitution of Co for Fe in FINEMET and Nb-containing HITPERM alloys

J S Blázquez[1], J M Borrego[1], C F Conde[1,3], A Conde[1] and J M Greneche[2]

[1] Departamento de Física de la Materia Condensada, Instituto de Ciencia de Materiales, CSIC, Universidad de Sevilla, PO Box 1065, 41080 Sevilla, Spain
[2] Laboratoire de Physique de l'Etat Condensé, UMR CNRS 6087, Université du Maine, F-72085 Le Mans Cedex 9, France

E-mail: conde@us.es (A Conde)

Received 19 February 2003, in final form 6 May 2003
Published 30 May 2003
Online at stacks.iop.org/JPhysCM/15/3957

Abstract

A comparative study of the effects of partial substitution of Co for Fe on thermal stability, crystallization and magnetic properties of Co-containing FINEMET and HITPERM alloys series is presented. The difference in metalloid and Nb content between the two alloy series and the presence of Si in the nanocrystals in the case of FINEMET alloys appear as key parameters. A recrystallization process involving the α-Fe type phase in nanocrystalline alloys of both series is evident from thermomagnetic results as a significant decrease in magnetization at the second crystallization stage.

1. Introduction

Nanocrystalline alloys obtained by primary crystallization of melt-spun amorphous Fe-based precursors exhibit an excellent soft magnetic behaviour due to their peculiar two-phase microstructure: nanosized Fe-rich ferromagnetic crystals embedded in a ferromagnetic amorphous matrix with a lower Curie temperature [1]. Since the grain size of the crystallites is smaller than the magnetic interaction length, the magnetocrystalline anisotropy is averaged out by exchange interactions [2, 3].

Several magnetic nanocomposite types of similar microstructure but different compositions have been developed: FeSiBCuNb alloys [4], known up to now as FINEMET, FeMB(Cu) (M = Zr, Nb, Hf) alloys [5, 6], called NANOPERM, and, more recently, (FeCo)MB(Cu) alloys [7], called HITPERM. The two former compositions (FINEMET and NANOPERM) are among the softer magnetic materials known at room temperature. However, at temperatures above the Curie temperature of the residual amorphous phase, the outstanding magnetic properties are lost and their applicability cannot be extended over ∼600 K. Partial

[3] Author to whom any correspondence should be addressed.

0953-8984/03/233957+12$30.00

substitution of Co for Fe in HITPERM alloys improves their applicability at high temperatures due to the higher saturation magnetization and Curie temperature of the crystalline and amorphous phases [8, 9]. Co-containing FINEMET alloys have also been studied [10–15].

Nanocrystallization on FINEMET and HITPERM alloys has been revised recently in several papers [1, 16, 17]. Cu addition is revealed as necessary to achieve the best nanocrystalline microstructure in FINEMET alloys [18]: clustering of Cu atoms in the preliminary stages of crystallization catalyzes the nucleation of α-Fe, Si primary crystals. However, in the case of NANOPERM and HITPERM alloys, the nanocrystalline microstructure can be obtained in Cu-free alloys. The role of Nb (Zr, Hf) is to hinder the grain growth due to its partition to the grain boundaries because of its very low solubility in the forming crystalline phase and its slow diffusivity.

The data from the literature reveal some differences in the role of Cu for Nb- and Zr-containing HITPERM alloys in the nanocrystallization process. For Nb-containing alloys, Cu produces a refinement of the microstructure [19] in a similar way as that observed for NANOPERM alloys. However, for Zr-containing alloys, Cu shows no significant influence, which has been attributed to the absence of Cu clustering during the precrystallization stage [20]. In fact, for the HITPERM alloy of composition $Fe_{44}Co_{44}Zr_7B_4Cu_1$, Cu clustering is not observed and Cu atoms are homogeneously distributed in the amorphous matrix [20]. On the other hand, for the Nb-containing HITPERM alloy of composition $Fe_{39}Co_{39}Nb_6B_{15}Cu_1$ atom–probe (3DAP) results clearly reveal the formation of Cu clusters [21]. For FINEMET alloys, substitution of Co for Fe provokes a decrease of the driving force for Cu clustering as Co concentration in the alloy increases [12].

These results seem to indicate that, in Co-containing nanocrystalline alloys, Cu clustering is a complex phenomenon, affected by different parameters, e.g. Co content, type and content of early transition metals and mixing enthalpies between the different elements in the alloy. The composition of Nb-containing HITPERM alloys is closer to FINEMET alloys than that of a classical $Fe_{44}Co_{44}Zr_7B_4Cu_1$ HITPERM alloy, with Si appearing to be the only non-common element. This fact simplifies the comparison.

Although several studies have been devoted to Nb-containing HITPERM [19, 21–29] and Co-FINEMET alloys [10–15] separately, a detailed comparative study showing the common mechanisms of the nanocrystallization phenomenon of the α-Fe, Co(Si) phase is missing. In this work, this study is performed in terms of their microstructure and magnetic properties. In addition high temperature transformations (recrystallization process) and the final products of the devitrification process have been compared. Different experimental techniques, including differential scanning calorimetry (DSC), thermomagnetic gravimetry (TMG), x-ray diffraction (XRD), transmission electron microscopy (TEM) and Mössbauer spectrometry (MS) have been used in a combined way.

2. Experimental procedure

Amorphous ribbons, ∼5 mm wide and 15–25 μm thick, of nominal composition $Fe_{73.5-x}Co_xSi_{13.5}B_9Cu_1Nb_3$ ($x = 0$, 13.5 and 60 at.% Co) and $Fe_{78-x}Co_xNb_6B_{15}Cu_1$ ($x = 18$, 39 and 60 at.% Co) were obtained by a single roller melt-spinning technique. DSC curves were recorded by a Perkin-Elmer DSC-7 in order to observe the devitrification processes. TEM (Philips CM200; 200 kV) and XRD (Siemens, D5000 patterns with Cu Kα radiation) were used to study the microstructure of nanocrystalline and fully crystallized samples. The temperature dependence of magnetization was observed from TMG measurements performed in a thermobalance (Perkin-Elmer TGA-7) with the magnetic field of a small magnet (∼15 mT) applied to the sample. Mössbauer spectra were taken at room temperature in a transmission

Table 1. Crystallization onset temperatures, T_o, peak temperatures, T_p, and crystallization enthalpies, ΔH, of the two crystallization steps at a heating rate of 0.17 K s^{-1}, activation energy E_a and Avrami index, n, of the nanocrystallization process for $Fe_{73.5-x}Co_xSi_{13.5}B_9Nb_3Cu_1$ ($x = 0, 13.5, 60$ at.% Co) and $Fe_{78-x}Co_xB_{15}Nb_6Cu_1$ ($x = 18, 39, 60$ at.% Co) amorphous alloys.

Alloy x	T_o (K) ±0.5	T_{P1} (K) ±0.5	ΔH_1 (J g^{-1}) ±5%	E_a (eV) ±0.2	n ±0.2	T_{P2} (K) ±0.5	ΔH_2 (J g^{-1}) ±5%
			FINEMET				
0	791	813	70	4.1	0.7	961	17
13.5	805	825	102	4.5	0.9	967	34
60	754	769	87	3.8	1.0	909	40
			HITPERM				
18	728	761	101	3.6	0.5	987	11
39	716	739	108	3.6	0.6	969	28
60	694	736	61	3.1	0.6	907	60

geometry using a ^{57}Co (Rh) source, with the γ-beam perpendicular to the ribbon plane. The values of hyperfine parameters were refined using NORMOS [30] and MOSFIT [31] programmes. Thermal treatment of the samples for XRD, TEM, TMG and MS studies were performed under an Ar atmosphere in a halogen lamp furnace.

3. Results and discussion

3.1. Thermal stability

The devitrification process of the two studied alloy series occurs in two main stages, shown by the corresponding exothermic peaks. Figure 1 shows, as an example, DSC scans of $x = 13.5$ and 60 at.% Co FINEMET alloys and $x = 18$ and 60 at.% Co HITPERM alloys. The crystallization parameters are summarized in table 1 [11, 22]. For Co-containing alloys, the thermal stability of both as-cast amorphous and nanocrystalline alloys decreases as the Co content of the alloy increases. However, a slight increase of the crystallization onset temperature was observed in the low Co content FINEMET alloy compared to that of Co-free FINEMET alloy. The comparison of crystallization parameters of FINEMET and HITPERM alloys, for similar Co content, reveals that as-cast amorphous and nanocrystalline alloys of the first type series are more stable in temperature than those of the last one. This result can be ascribed to a higher metalloid and Nb content in FINEMET-type alloys (25.5 at.%), compared to that in HITPERM alloys (21 at.%), as these elements stabilize the initial and residual amorphous matrix.

The kinetics of the nanocrystallization process is slowed down in HITPERM alloys compared to that of FINEMET alloys, as shown by a lower Avrami exponent [11, 23]. This result can be attributed to the higher Nb content of HITPERM alloys compared to that of FINEMET alloys (6 and 3 at.%, respectively), as this element, insoluble in the crystalline phase and with a very low diffusivity, hinders the growth of the crystallites. This argument can be understood using a very simple model. The total surface of the nanocrystal is compared to that occupied by the Nb atoms which, due to their very low diffusivity, are supposed to remain at the nanocrystal surface after being rejected from the nanocrystal volume. As the nanocrystal surface grows as $\langle D\rangle^2$ ($\langle D\rangle$ is the mean grain size of the crystallite) and that occupied by Nb as $\langle D\rangle^3$ (amount of Nb atoms initially contained in the volume of the nanocrystal), the intersection

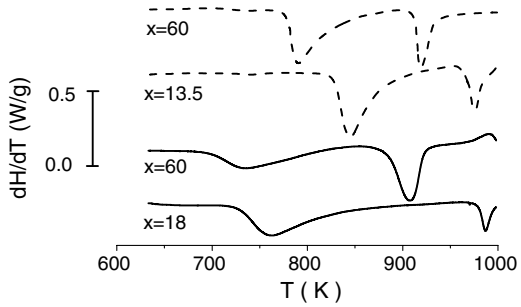

Figure 1. DSC scans at 0.17 K s^{-1} of as-quenched FINEMET (broken curves) and HITPERM (full curves) alloys.

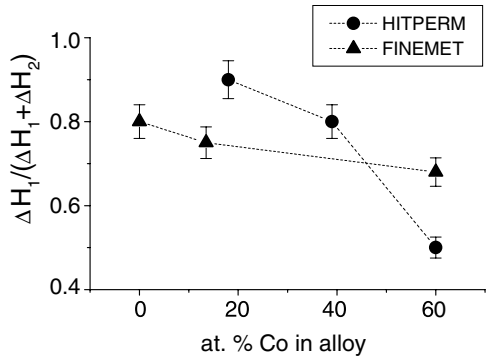

Figure 2. Enthalpy fraction of the first stage, $\Delta H_1/(\Delta H_1 + \Delta H_2)$, as a function of the Co content for as-quenched FINEMET and HITPERM alloys.

between both curves occurs at a lower crystalline diameter in the case of HITPERM (6 at.% of Nb) alloys than in the case of FINEMET (3 at.% of Nb) alloys, i.e. ∼12 and ∼23 nm, respectively. These values would be lowered if the nanocrystal surface occupied by B atoms were also considered.

This model implies a limit to the spherical growth of the nanocrystals, which is also in agreement with the microstructure observed for FINEMET and HITPERM alloys [11, 19]. In fact, for Cu-free HITPERM alloys, larger crystal sizes (up to 20 nm) compared to Cu-containing HITPERM alloys (∼5 nm) were found. However, these larger crystals present a very irregular shape, which can be described as groups of spherical nanocrystals about 5 nm in size with the same crystallographic orientation [19].

The enthalpy fraction of the first crystallization stage, defined as $\Delta H_1/(\Delta H_1 + \Delta H_2)$, where ΔH_1 and ΔH_2 are the enthalpies involved in the first and second crystallization stages, respectively, is shown in figure 2. A monotonic decrease of this enthalpy fraction can be observed as the Co content of the alloy increases for both alloy series, being the values corresponding to FINEMET alloys lower than those of HITPERM alloys for low Co content alloys but higher for alloys with 60 at.% Co content.

The enthalpy fraction at the DSC peak temperature, T_p, relative to that of the total nanocrystallization process, $\Delta H(T_p)/\Delta H_1$, decreases monotonically as the Co content increases in the case of FINEMET alloys (values found are 0.35, 0.30 and 0.20 for $x = 0$, 13.5 and 60 at.% Co, respectively). The value of $\Delta H(T_p)/\Delta H_1$ can be considered as an estimate of the relative contribution of the early stages of the nanocrystallization process, where nucleation

of the Fe(Co)Si phase is more important. Therefore, a decreasing value of $\Delta H(T_p)/\Delta H_1$ as Co content increases in FINEMET-type alloys series is in agreement with the observed decrease of the driving force for Cu clustering for increasing Co content in the alloy [12], as Cu clusters are the sites for heterogeneous nucleation in FINEMET alloys. However, similar values of $\Delta H(T_p)/\Delta H_1$, around 0.30, were found in HITPERM alloys irrespective of the Co content of the alloy. This result is in agreement with the fact that, in Nb-containing HITPERM alloys with $x = 39$ at.% Co, no preferential rejection of Fe atoms from the Cu clusters compared to that of Co atoms was detected, and the concentrations of Fe and Co atoms in the Cu clusters were found to be the same, ∼29 at.% [21].

3.2. Nanocrystalline microstructure

The microstructure of both alloy series at the end of the nanocrystallization process, consisting of α-Fe(Co), Si and α-Fe, Co grains for FINEMET and HITPERM-type alloys series, respectively, embedded in a residual amorphous matrix, is compared in terms of the relevant parameters, i.e. lattice parameter, crystal size and crystalline volume fraction.

The composition of the nanocrystals in the case of FINEMET-type alloys was determined on the basis of combined structural and magnetic data [13]. From Mössbauer spectra, the Si content of the nanograins was estimated from the number of Fe sites and the proportion of each Fe component corresponding to the crystalline phase. The Fe atomic fraction was calculated from the crystalline and amorphous absorption areas of Mössbauer spectra, assuming the same recoilless factor for both phases. The content (atomic fraction) of element i in the crystalline phase, $\langle C_i \rangle_{cr}$, was calculated from a simple balance equation:

$$\langle C_i \rangle_{cr} = [\langle C_i \rangle - (1 - x_C)\langle C_i \rangle_{am}]/x_C \tag{1}$$

where x_C is the crystalline volume fraction obtained from x-ray diffractograms, $\langle C_i \rangle$ is the average concentration of the element i of the alloy and $\langle C_i \rangle_{am}$ is the content of element i in the amorphous phase. The compositions determined for the nanocrystals are $Fe_{80}Si_{20}$, $Fe_{68.5}Co_{13.5}Si_{18}$ and $Fe_{35}Co_{60}Si_5$ for $x = 0$, 13.5 and 60 at.% Co, respectively [13]. Therefore, partitioning of Co during nanocrystallization shows a homogeneous distribution of this element throughout the nanocrystals and the amorphous matrix. A homogeneous distribution of Co was also found in HITPERM alloys from 3DAP experiments [21]. This result allows a straightforward derivation of the composition of nanocrystals in the case of HITPERM alloys, assuming only Fe and Co atoms inside the crystals: $Fe_{82}Co_{18}$, $Fe_{61}Co_{39}$ and $Fe_{40}Co_{60}$ for $x = 18$, 39 and 60 at.% Co, respectively.

Figure 3 shows the dependence of the lattice parameter, a, of the crystalline phase (calculated from the angular position of the first four XRD maxima) as a function of the Co content for both alloy series. A decrease of a as Co content increases can be observed, following the same behaviour as that found in Fe,Co crystalline binary alloys [32], whose values are also shown in figure 3 for comparison. Values of a corresponding to FINEMET alloys are lower than those of HITPERM alloys due to the Si content of the nanocrystals. Values of Si content of the nanocrystals obtained from a data confirm those obtained from Mössbauer analysis [13].

The mean grain size of the nanocrystals, $\langle D \rangle$, obtained from TEM images (table 2) increases with Co content (from ∼10 to ∼20 nm) [11] in FINEMET alloy series, whereas it remains constant (∼5 nm) [19] in HITPERM alloy series. This result is in agreement with the proposed decrease of the driving force of Cu clustering for FINEMET alloys. In fact, the lower the number density of Cu clusters, the lower the number of nucleation sites for emerging Fe(Co),Si nanocrystals is and, therefore, the larger the average distance between them. This

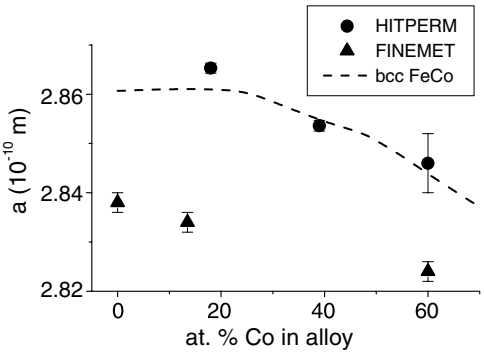

Figure 3. Lattice parameter of the FeCo(Si) phase as a function of the Co content for FINEMET and HITPERM alloys at the end of the nanocrystallization process. For comparison the curve corresponding to bcc FeCo binary alloys is shown.

Table 2. Crystalline volume fraction and grain size of the nanocrystals at the end of the nanocrystallization process for $Fe_{73.5-x}Co_xSi_{13.5}B_9Nb_3Cu_1$ ($x = 0$, 13.5, 60 at.% Co) and $Fe_{78-x}Co_xB_{15}Nb_6Cu_1$ ($x = 18$, 39, 60 at.% Co) nanocrystalline alloys.

FINEMET x	x_C(%) ±5	$\langle D\rangle$ (nm) ±5	HITPERM x	x_C(%) ±5	$\langle D\rangle$ (nm) ±5
0	65	10	18	54	5
13.5	60	12	39	53	5
60	40	22	60	43	5

fact favours a larger grain size due to both less impingement between neighbouring crystals during the growth process and a larger region not depleted in Fe around the crystal.

The volume fraction of the nanocrystalline phase was obtained from the XRD integral intensity of the (110) reflection of the crystalline phase and that of the first diffuse maximum of the amorphous phase fitted by pseudo-Voigt functions. The area ratio was corrected taking into account the different scattering powers of amorphous and nanocrystalline phases. This correction is very important in the case of HITPERM alloys [24] but gives no significant changes in the case of FINEMET alloys due to the presence of Si in the nanocrystals, which is a light atom compared to Fe and Co and reduces the difference between the scattering powers of the average atom of the nanocrystalline grains and the residual amorphous phase. In HITPERM-type alloy series the higher content of B atoms, insoluble in the Fe-rich crystalline phase, also enhances the difference between the scattering powers of crystalline and amorphous phases, the latter being more enriched in light atoms.

The crystalline volume fraction achieved at the end of the nanocrystallization process in the case of alloys with lower Co content is higher in FINEMET alloys (∼65%, for $x = 0$ and 13.5 at.% Co) than in HITPERM alloys (∼55%, for $x = 18$ and 39 at.% Co). This difference could be attributed to the Si content in the nanograins in FINEMET-type alloy series. For $x = 60$ at.% Co of both alloy series, the crystalline volume fraction is significantly lowered, being limited to about 40% in the case of FINEMET-type alloys and to about 45% in the case of HITPERM-type alloys. This difference can be explained assuming that the Fe exhaustion of the amorphous matrix stops the nanocrystallization process. Effectively, if the Fe content of the residual amorphous matrix is calculated from the balance equation (1), the theoretical limit values obtained for x_C are 39 and 45% for $x = 60$ at.% Co FINEMET and HITPERM alloys, respectively. Therefore, whereas for low Co content FINEMET alloys a larger amount

of soluble atoms in the crystalline phase yields a larger crystalline volume fraction for this alloy series compared to that of the HITPERM alloy series, for 60 at.% Co-containing alloys the impoverishment in Fe is stronger in FINEMET alloys, yielding a lower value of x_C.

As was pointed above, from MS it is possible to obtain the fraction of probe atoms (Fe) in the different phases. If the composition of the nanocrystals is known, the crystalline atomic fraction, A_C, can be calculated. The relationship between A_C and x_C is direct if the average atomic size for the different phases can be considered equal (as in the case of FINEMET). However, in the case of HITPERM alloys, the high content of B (small atom which partitions to the amorphous matrix) makes it necessary to consider the effect of the different average atomic sizes for the amorphous matrix and the nanocrystals [25]. Besides this difficulty, the contribution of the interface to the crystalline volume fraction has to be taken into account. At the end of the nanocrystallization process, the fraction of Fe atoms in crystalline contribution is between 75 and 80% in the case of FINEMET alloys, increasing with Co content [13]. In the case of HITPERM alloys, the fraction of Fe atoms in the pure crystalline region is between 50 and 70%. These values increase up to 60–80% once the interface contribution is considered [25]. A detailed study of the comparison of crystalline volume fraction obtained from XRD and MS techniques is reported in [25] for the case of HITPERM alloys. In the case of FINEMET alloys, the crystalline volume fraction from XRD, the fraction of Fe atoms and the estimated Si content of the crystalline phase, allowed us to conclude, through the balance equation (1), a homogeneous distribution of Co throughout the amorphous matrix and the nanocrystals [13].

A comparison of crystalline volume fractions, x_C, obtained from XRD analysis and enthalpy fractions, calculated as $\Delta H_1/(\Delta H_1 + \Delta H_2)$ from DSC measurements, as a function of Co content leads to a qualitative agreement in both alloy series: both quantities decrease as Co content increases. However, for $x = 60$ at.% Co alloys the decrease in enthalpy fraction is lower in FINEMET alloys than in HITPERM alloys, whereas a similar decrease in x_C is found for both alloy series. This result could be partially ascribed to a decrease of the driving force for Cu clustering with increasing Co content and supports the idea that the driving force for Cu clustering does not decrease so strongly in the case of Nb-containing HITPERM alloys [21] as it does for FINEMET [12] and Zr-containing HITPERM alloys [20]. In fact, as the number density of the Cu cluster decreases, the formation of crystals might be energetically less favourable and therefore the enthalpy per unit of transformed volume might increase as the Co content increases in the case of FINEMET alloys.

3.3. Magnetic properties

The comparative study of the magnetic properties of the two alloy series studied is discussed in terms of their hyperfine parameters and Curie temperatures.

Mössbauer spectra of as-quenched samples were fitted using a discrete hyperfine magnetic field distribution, $P(B)$, typical of the amorphous structure. The average hyperfine magnetic field of the as-cast amorphous phase increases with increasing Co content in both alloy series as is shown in figure 4. Values corresponding to HITPERM samples are larger than those of FINEMET ones, in agreement with their larger amount of magnetic atoms (Co and Fe).

Mössbauer spectra and hyperfine magnetic field distributions for as-quenched samples of FINEMET alloys with $x = 13.5$ and 60 at.% Co and HITPERM alloys with $x = 18$ and 60 at.% Co are shown in figure 5. In the case of 60 at.% Co alloys of both series, the presence of an intense peak around 25 T and a smaller peak at low hyperfine field values ($\sim$10 T) can clearly be observed. However, for low Co content alloys (18 and 13.5 at.% Co) this 'double peak' structure is not well defined, mainly due to the broadening of the main peak as the Co content

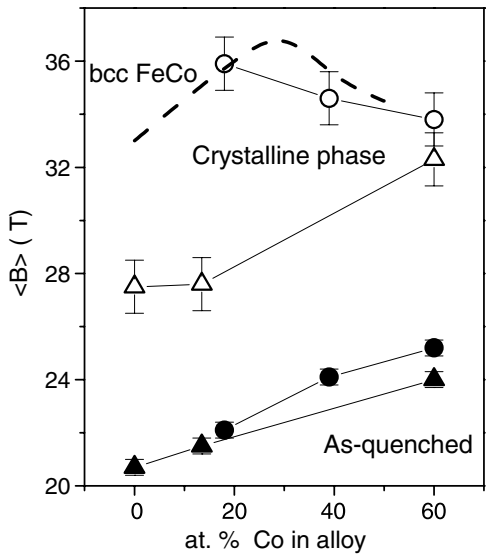

Figure 4. Average hyperfine magnetic field of as-quenched alloys and FeCo(Si) phase of nanocrystalline samples for HITPERM (circles) and FINEMET (triangles) alloys as a function of the Co content of the alloy. For comparison the curve corresponding to bcc FeCo binary alloys is shown.

decreases in the alloy. This effect, also detected in FeCoB [33] and FeCoSiB alloys [34–36], could be ascribed to a decrease of the short-range order around Fe atoms, although other effects can also affect the broadening of the distribution. In fact, for bcc FeCo alloys, the slope of the curve of the average hyperfine magnetic field versus Co content at low Co content (from 0 to 30 at.%) is larger than that for high Co content (>50 at.%) [37]. Consequently, in the case of low Co content alloys the same standard deviation of the composition would lead to a larger standard deviation of the hyperfine magnetic field compared to that of high Co content alloys. The effect of Si content on the average hyperfine magnetic field and the broadening of the distribution increases with the Co content of the alloy, in agreement with previous results on FeCoSiB amorphous alloys [36].

The low field peak ($\sim$10 T) can be ascribed to the presence of Nb atoms in the neighbourhood of Fe atoms, as no evidence of such low values are found in FeCo(Si)B metallic glasses [33–36]. The relative percentage of this peak to the total P(B) distribution is larger for 60 at.% Co HITPERM alloy compared to that of 60 at.% Co FINEMET alloy, in agreement with the Nb content of the alloys.

Mössbauer spectra of nanocrystalline samples exhibit a complex hyperfine structure which, for HITPERM alloys, can be described in terms of three regions: crystalline, amorphous and interface [25]. In the case of FINEMET alloys, the presence of Si inside the nanocrystalline grains originates the appearance of low field crystalline contributions that overlap with the amorphous and/or interface contributions. Consequently, the interface contribution is not clearly resolved in FINEMET-type alloys [13, 38].

The average hyperfine magnetic field of the crystalline phase increases with Co content in nanocrystalline FINEMET samples whereas the opposite tendency is found for HITPERM ones, as can be observed in figure 4. This different behaviour can be understood considering the values corresponding to the bcc Fe,Co disordered phase in the binary alloy, also included in figure 4. The average hyperfine magnetic fields of HITPERM-type alloy series are close

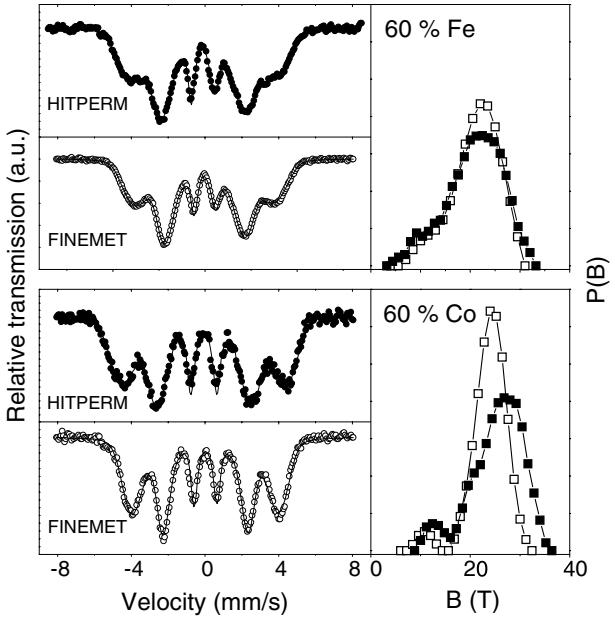

Figure 5. Mössbauer spectra and hyperfine magnetic field distribution for as-cast samples of FINEMET with $x = 13.5$ and HITPERM with $x = 18$ at.% Co alloys (above), and FINEMET and HITPERM with $x = 60$ at.% Co alloys (below).

to those of the binary alloy. The lower values found for $x = 39$ and 60 at.% Co HITPERM alloys, compared to those of the binary alloy, could be ascribed to a certain degree of order of the crystalline phase (α'-Fe, Co) [25]. The significantly lower values of hyperfine magnetic field for FINEMET samples are due to the presence of Si in the nanocrystals. The larger average hyperfine magnetic field corresponding to $x = 60$ at.% Co FINEMET alloy compared to values for $x = 0$ and 13.5 at.% Co is a consequence of the lower Si content in the crystalline phase for this composition.

Figure 6 shows thermomagnetic plots at 0.67 K s^{-1} of FINEMET and HITPERM as-quenched alloys. In the case of HITPERM-type alloy series, the Curie temperature, T_C, of the 18 at.% Co sample is 625 K, whereas for the alloys with higher Co content the fall in magnetization, M, due to the ferro–paramagnetic transition overlaps with the increase in M due to the emerging ferromagnetic Fe,Co nanocrystals. In the case of FINEMET-type alloys series, T_C of the as-quenched alloys are 590, 635 and 675 K for $x = 0$, 13.5 and 60 at.% Co, respectively [11].

The Curie temperature of the nanocrystals for Co-free FINEMET alloy is lower than the onset temperature of the second crystallization stage. Consequently, after the ferro–paramagnetic transition of the Fe,Si crystals, the system becomes paramagnetic and no signal is registered by TMG measurements. Only after the onset of the second transformation stage can small deviations from zero, ascribed to the formation of a small amount of a Fe_2B phase with higher Curie temperature [39], be observed. In contrast, for Co-containing alloys of both series, the Curie temperature of the nanocrystals is higher than that of the onset of the second crystallization process. The observed fall in magnetization at the temperature range of the second crystallization process shows a recrystallization involving Fe,Co(Si) crystals as will be described in the next section. At higher temperatures, for FINEMET-type alloys the magnetization reaches a zero value at 875, 1020 and 1030 K for $x = 0$, 13.5 and 60 at.% Co,

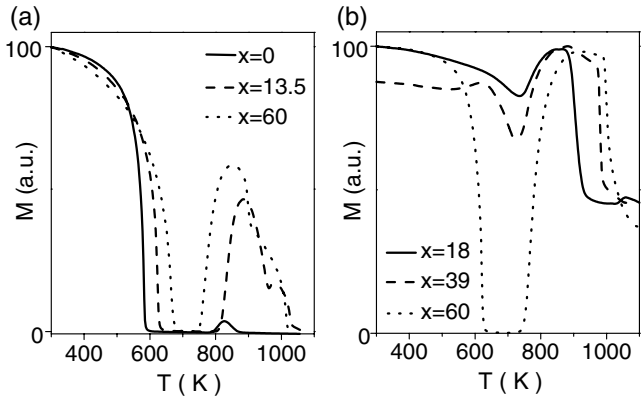

Figure 6. Thermomagnetic plots, at 0.67 K s^{-1}, for as-quenched samples of FINEMET (a) and HITPERM (b) alloys.

respectively (figure 6(a)), indicating the Curie temperatures of the Fe,Co(Si) crystalline phase. For HITPERM alloys (figure 6(b)), samples remain ferromagnetic at the maximum explored temperature, denoting a higher Curie temperature of the Fe,Co crystals. The absence of Si in the grains in the case of HITPERM alloys increases their Curie temperature up to values above the explored temperature region. In fact, for binary alloys the structural transition from a α-Fe, Co phase to a γ-Fe, Co phase (at 1184 K) occurs at a lower temperature than the extrapolated Curie temperature of a α-Fe, Co phase for concentrations of Co higher than 15 at.% [40].

Curie temperatures given above for FINEMET samples correspond to the Fe(Co),Si phase after the second crystallization stage and, consequently, cannot be directly ascribed to those of the Fe(Co),Si nanocrystals, as compositional changes might occur during the recrystallization process. In fact, in Co-free FINEMET alloys changes in the Curie temperature of the Fe,Si phase after annealing at temperatures above the second transformation stage have been ascribed to a decrease in the Si content of the crystals [39].

3.4. Recrystallization process

An abrupt decrease of the magnetization is observed in all Co-containing alloys at the temperature range of the second DSC exotherm, as was pointed above. This feature was ascribed to a recrystallization process of a α-Fe, Co phase (ferromagnetic at T_{x2}) to a $Fe_{23}B_6$-type phase (paramagnetic at T_{x2}) in HITPERM-type series [26]. In the case of Co-free FINEMET alloys this recrystallization feature cannot be detected from TMG experiments as the T_C of the nanocrystalline grains is lower than T_{x2}. For Co-containing FINEMET alloys, a recrystallization process is also evident from TMG curves (figure 7). The shift of the temperature corresponding to the fall in magnetization with the heating rate, reflecting a thermally activated character, and the irreversibility of the magnetization change characterize without ambiguity this feature as a recrystallization process. The decrease in volume fraction, derived from XRD data, of Fe(Co),Si crystals after the second crystallization stage, corroborates a partial transformation of these crystals.

XRD and TEM results show an increasing amount of the boride phase along with an increasing size of the boride crystals as the Co content in the alloy increases for fully crystallized samples of both alloy series [11, 27]. These results would indicate a higher relevance of the recrystallization process in Co-rich alloys.

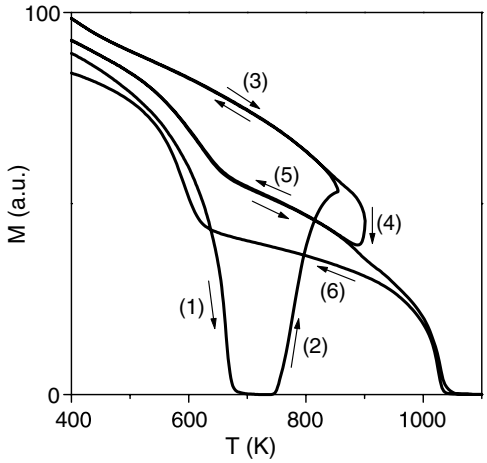

Figure 7. Thermomagnetic plots, at 0.67 K s^{-1}, on successive heating–cooling cycles for a $Fe_{13.5}Co_{60}Si_{13.5}B_9Nb_3Cu_1$ alloy.

4. Conclusions

The effects of the partial substitution of Co for Fe in FINEMET- and HITPERM-type alloys have been studied in terms of the differences in thermal stability, microstructure, magnetic properties and recrystallization processes.

- Thermal stability of the as-cast amorphous and nanocrystalline alloys decreases as the Co content increases in both alloy series.
- Nanocrystalline microstructure is strongly affected by the Nb content of the alloy.
- The presence of Si in the nanocrystals, in the case of FINEMET alloys, reduces the values of the lattice parameter and increases the crystalline volume fraction at the end of the nanocrystallization process of Fe-rich alloys when compared to Fe-rich HITPERM alloys. The exhaustion in Fe of the amorphous matrix reduces the final nanocrystalline volume fraction of 60 at.% Co alloys, when compared to Fe-rich ones in both alloy series.
- Curie temperatures and average hyperfine magnetic fields of the amorphous and crystalline phases are lower for FINEMET alloys than for HITPERM alloys due to the presence of Si.
- MS reveals a 'double peak' hyperfine magnetic field distribution for as-cast samples in both alloy series, being better resolved for Co-rich alloys.
- A recrystallization process in nanocrystalline alloys of both alloy series, involving Fe,Co(Si) crystals, is evident from thermomagnetic curves as a significant decrease in magnetization at the second crystallization stage. XRD results corroborate a decrease in the Fe,Co(Si) volume fraction.

Acknowledgments

This work was partially supported by the DGES of the Spanish Ministry of Science and Technology and EU-FEDER (Project MAT2001-3175), and by the PAI of the Junta de Andalucía. J S Blázquez acknowledges a research fellowship of the DGES.

References

[1] McHenry M E, Willard M A and Laughlin D E 1999 *Prog. Mater. Sci.* **44** 291
[2] Herzer G 1989 *IEEE Trans. Magn.* **25** 3327
[3] Hernando A, Vázquez M, Kulik T and Prados C 1995 *Phys. Rev.* B **51** 3581
[4] Yoshizawa Y, Oguma S and Yamauchi K 1988 *J. Appl. Phys.* **64** 6044
[5] Suzuki K, Kataoka N, Inoue A, Makino A and Masumoto T 1990 *Mater. Trans. JIM* **31** 743
[6] Suzuki K, Makino A, Kataoka N, Inoue A and Masumoto T 1991 *Mater. Trans. JIM* **32** 93
[7] Willard M A, Laughlin D E, McHenry M E, Thoma D, Sickafus K, Cross J O and Harris V G 1998 *J. Appl. Phys.* **84** 6773
[8] O'Handley R C 1999 *Modern Magnetic Materials: Principles and Applications* (New York: Wiley)
[9] Wijn H P J 1991 *Landolt-Börnstein: Magnetische Eigenschafen von Metallen* (Berlin: Springer)
[10] Müller M, Grahl H, Matter N, Kühn U and Schnell B 1996 *J. Magn. Magn. Mater.* **160** 284
[11] Conde C F and Conde A 1998 *Mater. Sci. Forum* **269–272** 719
[12] Ohnuma M, Hono K, Abe T, Onodera H, Linderoth S, Pedersen J S and Yoshizawa Y 2001 *Proc. 22nd Riso Int. Symp. on Materials Science: Science of Metastable and Nanocrystalline Alloys—Structure, Properties and Modelling (Roskilde, Denmark, 2001)* ed A R Dinesen, M Eldrup, D J Jensen, S Linderoth, T B Pedersen, N H Pryds, A S Pedersen and J A Wert (Roskilde: Riso National Laboratory) p 341
[13] Borrego J M, Conde C F, Conde A and Greneche J M 2002 *J. Phys.: Condens. Matter* **14** 883
[14] Gómez-Polo C, Marín P, Pascual L, Hernando A and Vázquez M 2002 *Phys. Rev.* B **65** 024433
[15] Gómez-Polo C, Pérez-Landazabal J I, Recarte V, Campo J, Marín P, López M, Hernando A and Vázquez M 2002 *Phys. Rev.* B **66** 012401
[16] Kemeny T, Kaptas D, Kiss L F, Balogh J, Vincze I, Szabo S and Beke D L 2000 *Hyperfine Interact.* **130** 181
[17] Kulik T 2001 *J. Non-Cryst. Solids* **287** 145
[18] Yoshizawa Y and Yamauchi K 1990 *Mater. Trans. JIM* **21** 307
[19] Blázquez J S, Franco V and Conde A 2002 *J. Phys.: Condens. Matter* **14** 11717
[20] Ping D H, Wu Y Q, Hono K, Willard M A, McHenry M E and Laughlin D E 2001 *Scr. Mater.* **45** 781
[21] Zhang Y, Blázquez J S, Conde A, Warren P J and Cerezo A 2003 *Mater. Sci. Eng.* A **353** 158
[22] Blázquez J S, Conde C F and Conde A 2001 *J. Non-Cryst. Solids* **287** 187
[23] Blázquez J S, Conde C F and Conde A 2003 *Appl. Phys.* A **76** 571
[24] Blázquez J S, Franco V, Conde C F and Conde A 2003 *J. Magn. Magn. Mater.* **254/255** 460
[25] Blázquez J S, Conde A and Grenèche J M 2002 *Appl. Phys. Lett.* **81** 1612
[26] Blázquez J S, Conde C F and Conde A 2001 *Appl. Phys. Lett.* **79** 2898
[27] Blázquez J S, Lozano-Pérez S and Conde A 2002 *Phil. Mag. Lett.* **82** 409
[28] Kane S N, Gupta A, Sarabhai S D and Kraus L 2003 *J. Magn. Magn. Mater.* **254/255** 495
[29] Zbroszczyk J, Olszewski J, Ciurzynska W, Wysocki B, Kolano R, Mynczyk A, Lukiewski M, Kolano A and Lelatko J 2003 *J. Magn. Magn. Mater.* **254/255** 513
[30] Brand R A, Lauer J and Herlach D M 1983 *J. Phys. F: Met. Phys.* **12** 675
[31] Teillet J and Varret F *MOSFIT Program* Université du Maine, unpublished
[32] Bozorth R M 1968 *Ferromagnetism* (Princeton, NJ: Van Nostrand-Reinhold)
[33] Gupta A, Kane S N, Kraus L and Duhaj P 1995 *J. Magn. Magn. Mater.* **140–144** 321
[34] Mostafa M A, Balough J and Kuzmann E 1986 *Phys. Status Solidi* a **96** 445
[35] Kopcewicz M, El Zayat M and Gonser U 1988 *J. Magn. Magn. Mater.* **72** 119
[36] Plazaola F, Orue I, Fernández-Gubieda M L and Barandiarán J M 1995 *J. Appl. Phys.* **77** 3338
[37] DeMayo B, Forester D W and Spooner S 1970 *J. Appl. Phys.* **41** 1319
[38] Grenèche J M, Miglierini M and Slawka-Waniewska A 2000 *Hyperfine Interact.* **126** 27
[39] Borrego J M, Conde C F and Conde A 2000 *Phil. Mag. Lett.* **80** 359
[40] Fernández-Guillermet A 1987 *High Temp.–High. Pressure* **19** 477